Journal of Structural Geology, Vol. 9, No. 8, pp. 935 to 953, 1987
Printed in Great Britain

0191-8141/87 $03.00 + 0.00

Fabric development in a fragment of Tethyan oceanic lithosphere from the Piemonte ophiolite nappe of the Western Alps, Valtournanche, Italy

W. Stefan Vogler

Mineralogisch-Petrographisches Institut, Universität zu Köln, Zülpicher Strasse 49, D-5000 Köln 1, F.R.G.

(*Received* 27 *March* 1986; *accepted in revised form* 1 *May* 1987)

Abstract—South of the Matterhorn the Valtournanche cuts through Alpine serpentinites, metagabbros, meta-pillowbasalts and metasediments—dismembered remnants of the Jurassic Tethyan oceanic crust, reassembled in the Piemonte ophiolite nappe. This study deals with a serpentinized ultramafic to mafic layered complex stemming from a spreading ridge environment. Cumulus fabrics of various kinds can be read through antigorite pseudomorphs, still allowing the detailed reconstruction of deep oceanic crust. Relics of igneous and metamorphic olivine prove crustal conditions during deformation. Fracturing of cumulus olivine was succeeded by plastic flow that activated low-temperature slip systems. Concomitant recrystallization produced metaperidotite only along shear zones, which are ascribed to subduction of the oceanic crust. At the turning point from subduction to obduction a static metamorphic event resulted in recovery and grain growth of recrystallized olivine. Afterwards serpentinization of the complex took place still under static conditions. Deformation of the serpentinite led to a sequence of four phases, involving non-penetrative cleavage formation, stretching and folding. This deformation is structurally related to obduction of the complex although partly accompanied by subduction zone metamorphism. Final movements of the ophiolites were due to cataclastic thrusting forming subnappe boundaries.

INTRODUCTION

The Piemonte ophiolite nappe of the Western Alps separates the underlying Pennine Monte Rosa/Gran Paradiso Nappe from the overlying Austro-Alpine Dent Blanche/Sesia Lanzo nappe system (Fig. 1). Both these nappes are made up of pre-Alpine continental crust, derived from the former northern (European) and southern (African) plates, respectively. Spreading of the Piemonte Ocean between these continents started in Jurassic time and ceased during late Cretaceous time, when compressional movements led to a S- to E-dipping subduction zone (Dal Piaz *et al.* 1972). This early-Alpine event was correlated with nappe formation (Gosso *et al.* 1979, Vogler 1984) and subduction zone metamorphism of various grades (Ernst & Dal Piaz, 1978, Chopin 1981). Deformation during subduction was simple. It commonly produced a dominant first cleavage and stretching lineation, whereas return of formerly subducted units did not cause penetrative deformation (Voll 1982). The late-Alpine event produced low-grade metamorphism in parts of the western Alpine arc, up to high-grade metamorphism within the Central Alps of Switzerland further east. The extreme flattening of deeply buried rocks in the Central Alps (Vogler & Voll 1981) is missing in the Austro-Alpine nappes of the Western Alps. There high-level deformation led to renewed nappe movements (Vogler 1984), at relatively low temperature, after the late-Alpine meta morphism.

The Piemonte ophiolite nappe is subdivided into the Combin zone on top and the Zermatt–Saas zone below (Fig. 1). The Combin zone contains Permo-Triassic to Liassic sediments and volcanics from an epicontinental shelf, which escaped subduction (Dal Piaz 1974). The Zermatt–Saas zone comprises some ophiolites (serpentinized ultramafics, metagabbros, pillow basalts and a thin Mesozoic sedimentary cover) of the Piemonte Ocean. This sequence has been subducted to a depth at which eclogite formed from basalt, still preserving the pillow structure (Bearth 1967). Eclogites were changed to glaucophane-amphibolites during their early-Alpine decompression. Late-Alpine metamorphism partly replaced high-pressure assemblages by greenschist-facies parageneses (Dal Piaz & Ernst 1978). The ultramafic rocks also passed through this tectono-metamorphic history.

The fragment of oceanic lithosphere studied is a part of the Zermatt–Saas zone, situated to the south of Breuil in the upper Valtournanche (Fig. 1), part of the Aosta Valley, Northern Italy. Round the village of Valtournanche the valley cuts the so called 'Gouffre de Busseraille serpentinite' (Bearth 1967, Gosso & Messiga 1977), which will be abbreviated to 'Gouffre serpentinite' in this article. Nearly 6 km^2 of serpentinite are exposed and nearly the same area to the south is covered by Quaternary deposits (Mattirolo 1912). One aim of this study was to compare the preserved magmatic fabrics, even after advanced serpentinization, to better preserved ophiolites. On the other hand Alpine deformational events have been studied with respect to number, kind and succession. This has been possible because relics of all evolutionary stages have been preserved; i.e. magmatic olivine, olivine that partly recrystallized during deformation or during static annealing, and antigorite pseudomorphs replacing all types of olivine. Arranging this complex structural association into a chronological order results in the following topics: (a) fabrics of magmatic origin; (b) deformational fabrics affecting the magmatic rocks; (c) fabrics of serpentinization; and (d) deformational fabrics affecting the serpentinite.

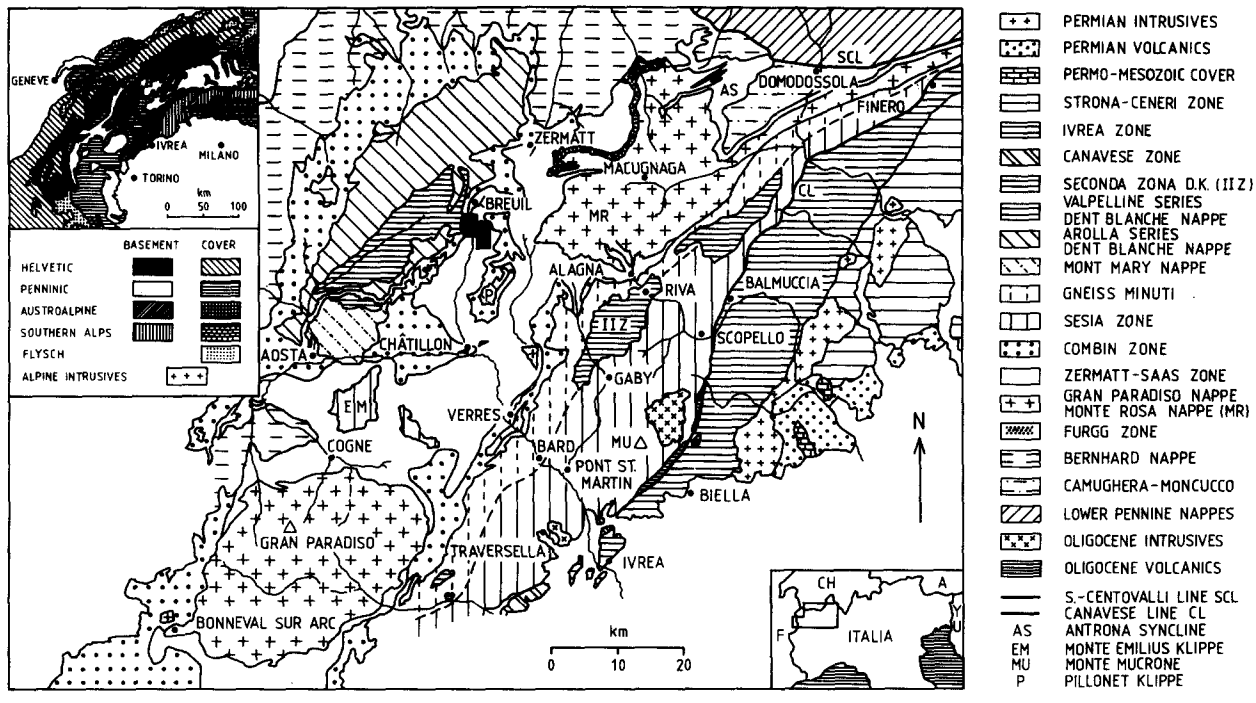

Fig. 1. Structural units of the Italian Northwestern Alps (after Hunziker 1974, Compagnoni *et al.* 1977). The studied area south of Breuil is marked in black (cf. Fig. 2). The inset shows a simplified geological map of the Western Alpine arc.

FABRICS OF MAGMATIC ORIGIN

One of the fundamental questions with respect to Alpine serpentinites is whether they are of mantle or crustal origin. The answer to this question will also illuminate the provenance of rocks that escaped complete subduction in this part of the Alpine chain. It thus may throw light on the mechanics involved in obduction processes.

Since serpentinization of the ultramafics was nearly complete and also mafic rocks were altered considerably during Alpine metamorphism, neither original composition of minerals, nor detailed cryptic variation trends could be established. Magmatic fabrics and petrology had to be deduced by means of various pseudomorphs found in serpentinites and metagabbros. However, the nomenclature of rocks, as used in the following sections, refers to the state before serpentinization (Streckeisen 1967), and the cumulus terminology follows Jackson (1967).

Field relations

Two different units build up the igneous complex: a lower ultramafic unit reaches *ca* 1800 m total thickness normal to the regional orientation of compositional layering. An upper mafic unit is exposed in tectonic and erosional remnants only, 70–120 m thick (Fig. 2). Both these values include rocks strongly flattened during the first deformation of the serpentinite (cf. D_1). They thus give only a minimum thickness for the original lithosphere incorporated in the Gouffre serpentinite.

Cumulate textures are the most striking primary fabrics that occur in the field. Here they will be analysed in some detail as they discriminate cumulate complexes from mantle slices (Coleman 1977, p. 90) and may be compared to better preserved ophiolites (e.g. Thayer 1969, Moores & Vine 1971, George 1978, Jacques 1981, Pallister & Hopson 1981), where they are ascribed to a mid-ocean spreading ridge environment.

Both units display a sometimes excellent fine-scale magmatic layering. It is defined by variation of modal composition and/or grain size and by preferred shape orientation of inequant crystals (Figs. 4a and 5f). The igneous layering dips gently N (~40°) (Fig. 3a), but locally is strongly tilted on short limbs of N-plunging third folds (Figs. 2 and 3g). Layered cumulate peridotite (primarily wehrlite and dunite), clinopyroxenite, chromitite and olivine chromitite conformably grade upward into layered cumulate gabbro, homogeneous gabbro and anorthosite. Lenses of cumulate gabbro, some tens of metres wide, are also intercalated in the peridotite. This succession of ultramafic and mafic cumulates is still the right way up.

Within the ultramafics, non-layered peridotites, whose olivine and clinopyroxene grain size varies from a few mm up to 20 mm, reach several metres in thickness. Where layering is found, it is a fine-scale rhythmic layering involving layers some cm to dm thick. Graded layers contain crystals 10 mm to less than 1 mm in size.

Streaks of chromitite, some mm to cm thick, are commonly conformably intercalated within the peridotite, pinching out after a few metres along strike. They may show modal graded transitions into olivine-chromitite at their top (Fig. 10). Euhedral grains of chrome spinel and magnetite are also randomly dispersed throughout the peridotite, reaching up to 6 mm across. Chrome spinel has also been enclosed in olivine. Parallel faces of both the encased and the encasing crystal (Fig. 4a) still reflect their adsorption along growth surfaces in

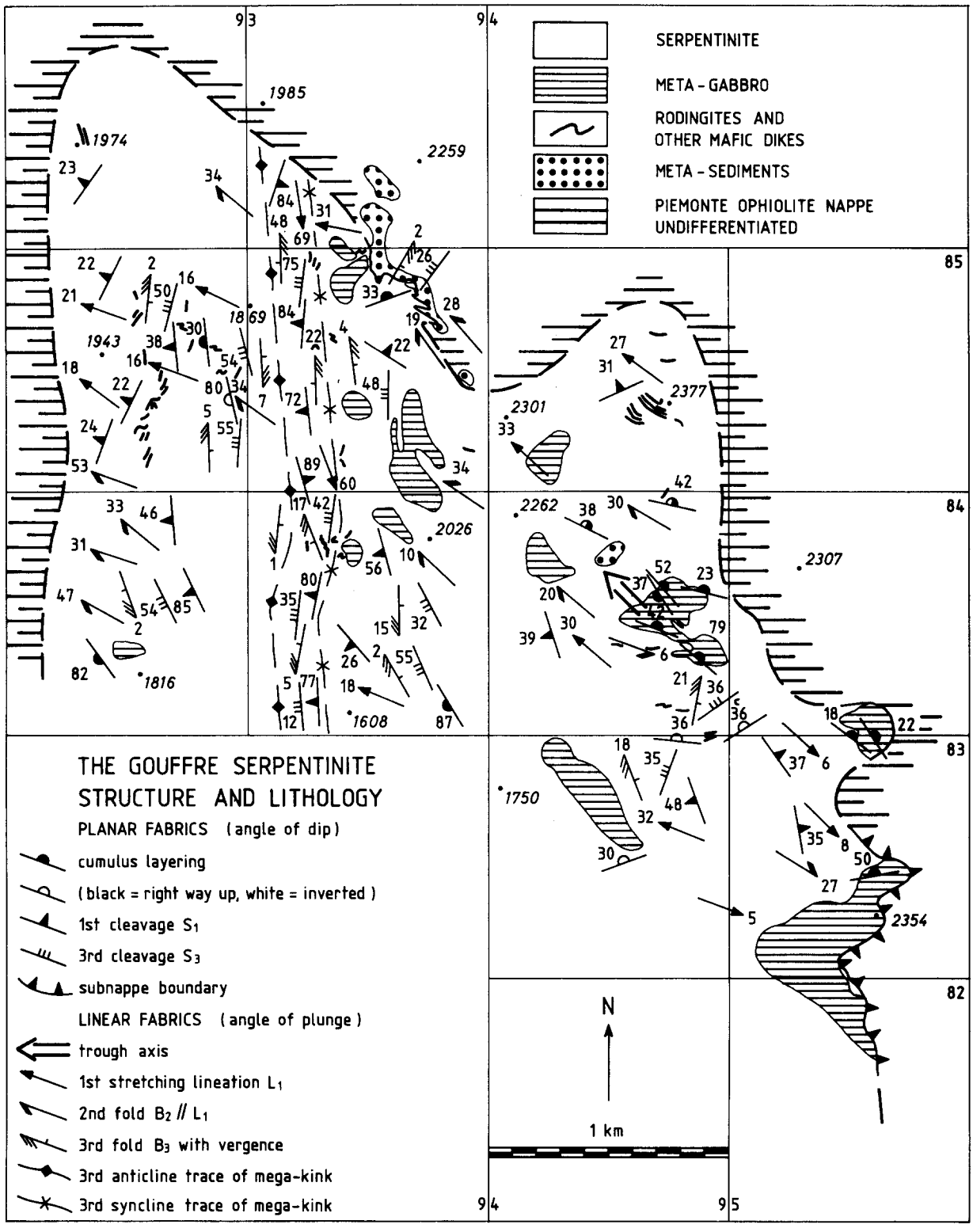

Fig. 2. Structure and lithology of the well exposed northern half of the Gouffre serpentinite. For location see Fig. 1.

the melt. Olivine and spinel in this case settled as a composite cluster, proving their simultaneous precipitation by fractional crystallization (Irvine 1975).

Cumulates rich in clinopyroxene occur as distinct layers of variable thickness between 1 and 50 cm. Boundaries against the peridotite are sharp. The grain size of clinopyroxene commonly ranges between 10 and 30 mm, rarely reaching 80 mm. Simple (100) growth twins are commonly found together with narrow (001) exsolution lamellae of orthopyroxene forming a herringbone texture (Fig. 5d). Grain size within graded pyroxenites is somewhat smaller, ranging from 10 to 2 mm. Magnetite fills the interstices of clinopyroxenites. Accessory zircons appear together with large apatite crystals for the first time.

No proof for the original presence of orthopyroxene has been found in the serpentinized peridotites. However, the occurrence of three different antigorite

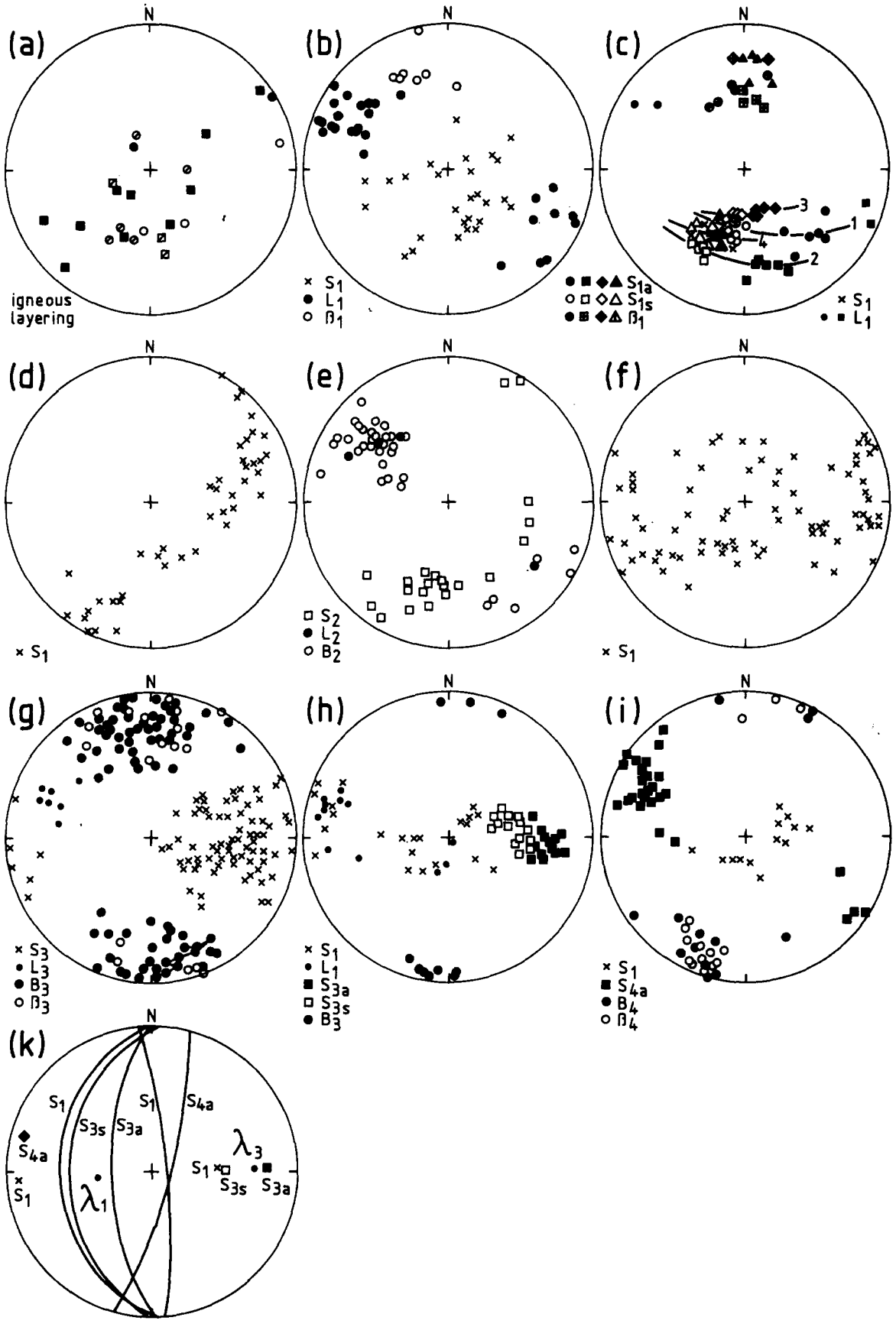

Fig. 3. Lower hemisphere equal-area projections of fabric elements from the Gouffre serpentinite and metagabbros. (a) Igneous layering, circles = serpentinite, squares = metagabbro. Full symbols denote upright, open symbols inverted layering, cross hatched symbols show no grading. (b) D_1: S_1, L_1 and β_1 (the layering–S_1 intersection line). (c) Four stages of progressive rotational D_1 (1–4) with antithetic S_{1a} and synthetic S_{1s} terminating in a single S_1. β_1 is S_{1a}–S_{1s} intersection line. (d) D_2: S_1 folded round second folds $B_2 \| L_1$. (e) D_2 fabric elements. (f) D_3: S_1 folded round third folds B_3. (g) D_3 fabric elements. β_3 is S_1–S_3 intersection line. A curved B_3-axis is followed through various attitudes of plunge. (h) D_3: fabric relations round a B_3 fold (cf. Fig. 10). (i) D_4 fabric elements, β_4 is S_1–S_4 intersection line. (k) D_3–D_4 transition due to progressive rotational deformation. A B_3 fold folding S_1 with a steep short limb and a W-dipping long limb is shown together with S_{3a} and S_{3s} and D_3-strain axes when S_{4a} makes its first appearance on the long limb of B_3.

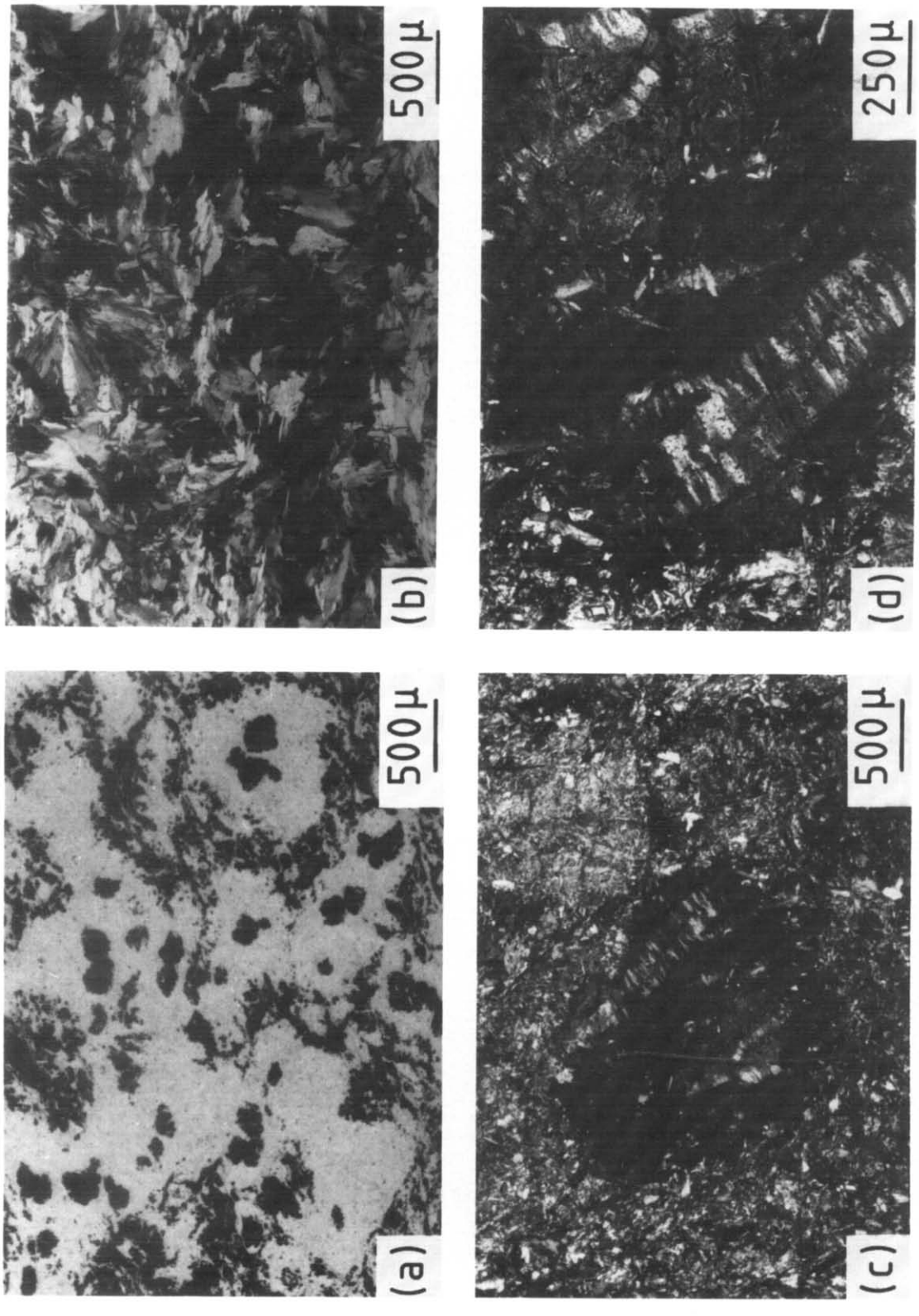

Fig. 4. (a) Serpentinized cumulus peridotite. Cluster of subhedral olivine (now light antigorite pseudomorphs) encasing euhedral spinel (now magnetite, black) accumulated to form igneous layering (EW). Interstitial chlorite and magnetite. (b) Interpenetrating texture of coarse antigorite after magmatic olivine. (c) Relict cumulus olivine (black and white) in a statically serpentinized matrix. The black crystal is shown in detail in (d). (d) Fractures healed by fibrous olivine (grey) and titanian clinohumite (white). Marginal antigorite replaced both magmatic and metamorphic olivine. *Continued* on p. 940.

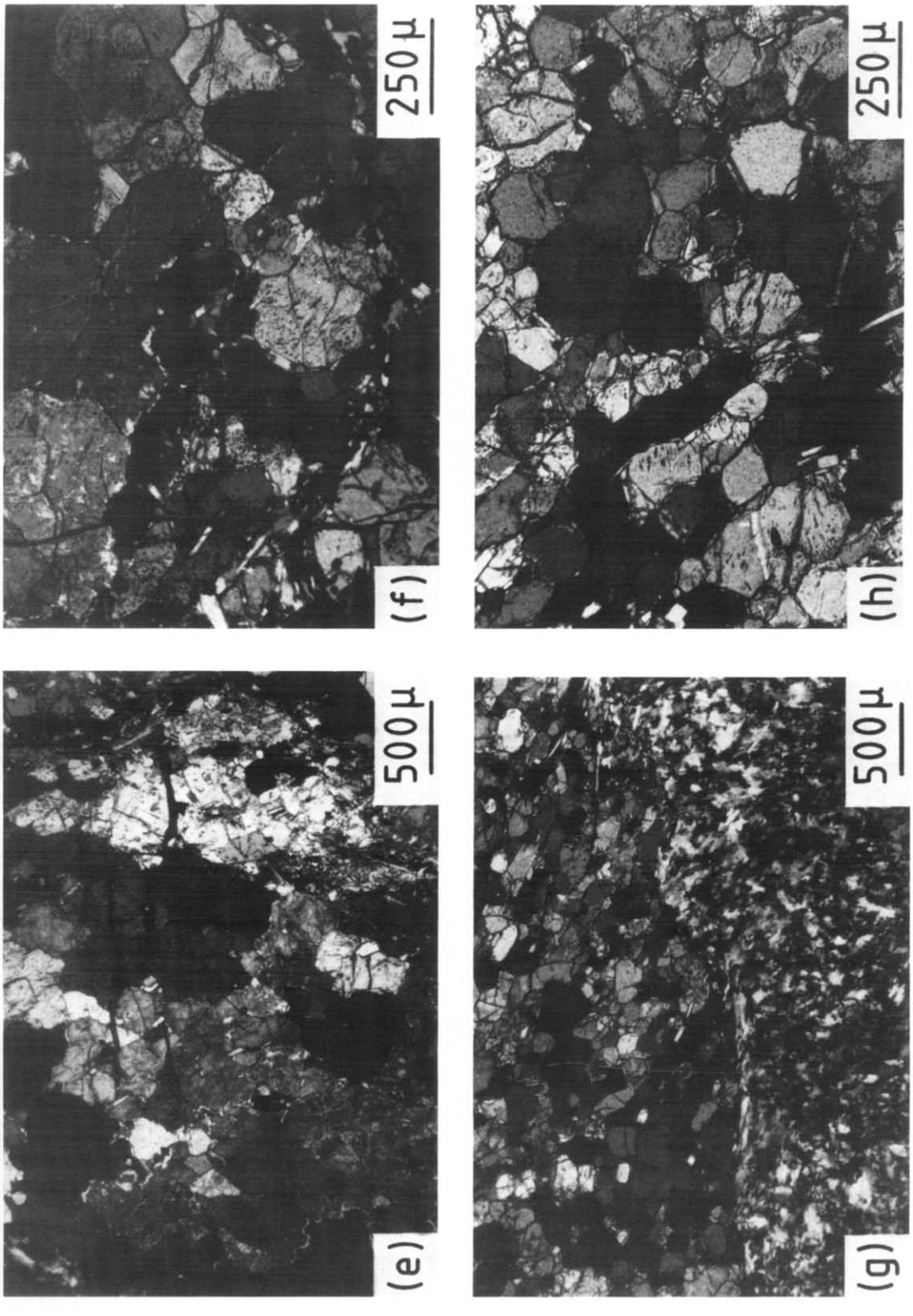

Fig. 4. *Continued*. (e) Dynamically recrystallized olivine (foliation NS) yielding the deformation texture of Fig. 6. (f) Tiny flakes of antigorite (white) growing along pre-existing grain boundaries of metamorphic olivine. (g) Equigranular annealing fabric of olivine replaced by an interlocking fabric of antigorite. Both fabrics trace back to static metamorphism. (h) Grain shape and grain-boundary distribution of olivine after grain growth (texture cf. Fig. 7). Equilibrium angles at triple points.

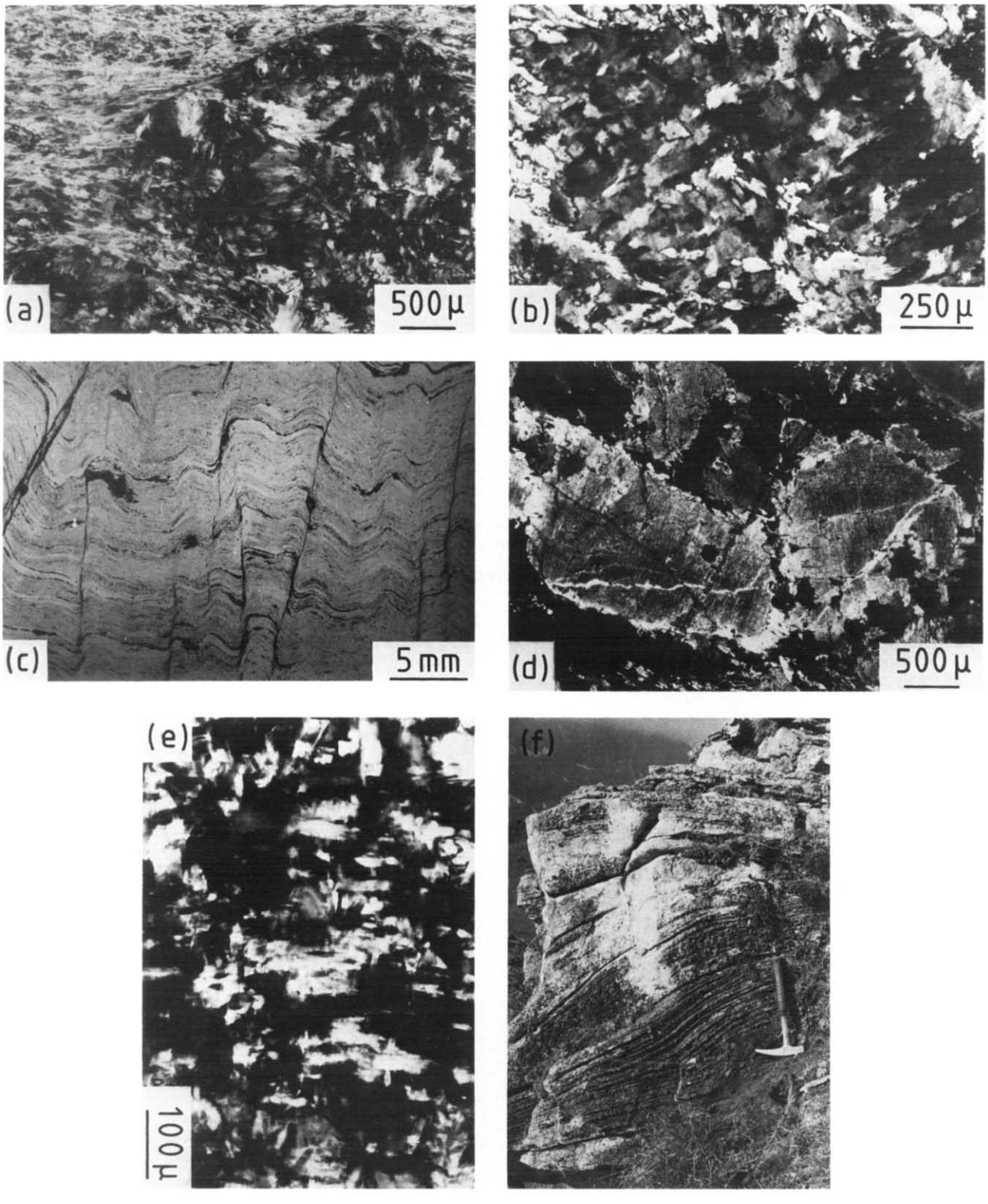

Fig. 5. (a) Antigorite schist encloses a rigid lenticular domain of interpenetrating antigorite lacking any plastic deformation. The boundary subparallel to S_1 is sharp showing no evidence of textural transition. The indistinct boundary normal to S_1 and L_1 goes back to schistose antigorite filling a pressure shadow to the left and partly replacing the older texture. (b) A strained antigorite bastite (dark background) parted into subgrains of low-angle orientation difference. Strong local distortion gave rise to nucleation of flaky cross-antigorite (white) with high angle boundaries against the parent grain. (c) Antigorite schist, S_1 and L_1 EW. Different tones of grey still correspond to different pseudomorphs of the flattened magmatic fabric (cf. Fig. 4a). Magnetite streaks after cumulus spinel. Detail from a B_3 fold hinge, where S_3 forms a conjugate system of widely spaced crenulation cleavages. Small S_{3s} shear zone to the left. (d) Magmatic crystals of brown clinopyroxene including narrow exsolution lamellae of orthopyroxene (serpentinized) have acquired colourless diopside rims during metamorphism. Interstitial magnetite. (e) The basal planes (EW) of an antigorite bastite (black) gently arch to the top after deformation. Recrystallization evolved through cross-antigorites (white) with basal planes nearly perpendicular to the parent grain. (f) Layered cumulates of the mafic unit. Flank of a depositional trough filled with anorthosite embedded in finely layered gabbros.

pseudomorphs at the same time may indicate that this mineral once formed as a cumulus or postcumulus phase.

Igneous layering and cumulus fabrics can be studied much more easily within the layered gabbro on top of the peridotite (Fig. 5f). The most common type shows a rhythmic alternation of nearly isomodal planar layers of gabbro rich in clinopyroxene with layers of gabbro rich in plagioclase. Rhythmically graded layering is common. Ratio grading is usually accompanied by size grading within a single layer. Modal proportions may vary from clinopyroxenite at the bottom to anorthosite at the top. Thickness of layers covers the cm- to dm-scope and reaches some metres for isomodal gabbros and anorthosites. Planar layers may be followed up to 20 m along strike, limited by outcrop dimensions.

Euhedral clinopyroxenes in gabbro are 10–80 mm long, sometimes down to 2 mm within graded layers. Clinopyroxene oikocrysts up to 150 mm across are rare.

Both post-cumulus and cumulus plagioclase occur. Cumulus plagioclase is euhedral and platy after (010), and may delineate a perfect shape orientation with (010) subparallel to layering, giving rise to cumulus planar lamination (Jackson 1967). Grain size commonly ranges between 2 and 30 mm.

Grading has been studied at 15 locations within both units (Figs. 2 and 3a). At four of these locations bedding is inverted, but at three of these this is due to recumbent isoclinal second folds. At the fourth point (to the west) a downward-facing size-graded clinopyroxenite contrasts with an upward-facing modal-graded olivine-chromitite in its neighbourhood. Thus all but one mineral- and size-graded layers indicate upright stratigraphy, already inferred from the succession of ultramafic and mafic rocks.

In addition the gabbros display cross-bedding structures at 12 places with partly size-graded clinopyroxenes. From these observations currents flowing towards the north can be deduced consistently. A trough filled with anorthosite is conformably interbedded between pyroxene-rich gabbro layers (Fig. 5f). Layers below the trough thin out toward the trough axis, which is gently plunging in a NW direction (Fig. 2). Persistence of planar layers on top of the trough clearly shows that the trough did not result from subsequent folding, but is a magmatic structure.

DEFORMATIONAL FABRICS AFFECTING THE MAGMATIC ROCKS

Where serpentinization was incomplete and subsequent deformation was lacking, cumulus olivine is exceptionally preserved. Euhedral to subhedral crystals, 2–7 mm long with typical small axial ratios ($\leq 2:1$) contribute to the cumulus texture. Their optic axial angle varies from $2V_z$ 84° to $2V_z$ 94° indicating Mg-rich compositions Fo_{95-75}. During the first stage of deformation cumulus olivines were bent and acquired undulatory extinction. Some were broken and extension fractures opened between their fragments. Broken crystals are healed by fibrous olivine and titanian clinohumite with their long axes parallel to an early stretching direction (Fig. 4d). Fragmentation occurred prior to serpentinization. This is proven by coarse interpenetrating antigorite growing at the expense of both magmatic and fracture-filling olivine (Fig. 4c). Brittle conditions can be deduced for the early stages of olivine deformation. The fissure filling process indicates the operation of a solution–redeposition mechanism concomitant to brittle deformation. Ramsay (1980) found such a crack–seal mechanism characteristic of rock deformation under crustal conditions not exceeding low-grade metamorphism. The same should be true for peridotites, taking into account the results of Ashby & Verrall (1977).

Some lenses of peridotite that escaped serpentinization and subsequent deformation show a texture of tectonic and metamorphic origin in remarkable contrast to the magmatic fabric. One may ask whether these rocks stem from upper mantle harzburgite tectonites commonly found at the basal section of ophiolites (Jackson *et al.* 1975, Ozawa 1983) or whether they were produced by plastic flow of metacumulates, i.e. by deformation of the igneous peridotites described so far. The conditions of plastic flow may help to answer this question. Two textural domains can be distinguished in thin section; one with a predominant deformation texture (porphyroclastic after Mercier & Nicolas 1975) the other with a pronounced annealing texture (equigranular mosaic texture of Mercier & Nicolas 1975). The deformation texture is made up of recrystallized olivine (Fig. 4e) with an average grain size of 3 mm, sometimes reaching 10 mm in length. Grain boundaries are strongly serrated and interlocking (Fig. 4f). The grains were flattened to axial ratios between 2:1 and 7:1. Titanian clinohumite of the same size and shape sometimes accompanies olivine. Aggregates of magnetite fragments form lenses completely embedded in olivine. They define a plane of flattening S and a stretching lineation L. Both were used as a structural reference system. Lattice preferred orientation of olivine has been studied to evaluate the predominant deformation mechanism. The fabric data were exclusively compiled from non-serpentinized regions of the specimen.

The deformation texture of olivine yields the following information (Fig. 6): obliquity between the textural components and the structural reference system is obvious. It is less pronounced for [001]. [001] displays a broad point maximum close to the spinel lineation L. Elongated in a plane normal to the foliation S it splits up into two submaxima. One [001]-submaximum coincides with L, the other deviates about 30° from L (Fig. 6b). This splitting seems to be characteristic for many metaperidotites of the Piemonte ophiolite nappe. [010] forms an irregular girdle normal to L. Several maxima in the girdle cluster round a low-density region producing a distorted small circle distribution. [100]-maxima also group round a low concentration area with remote resemblance to a small circle texture. Further weak maxima occur without any connection to a girdle. The main

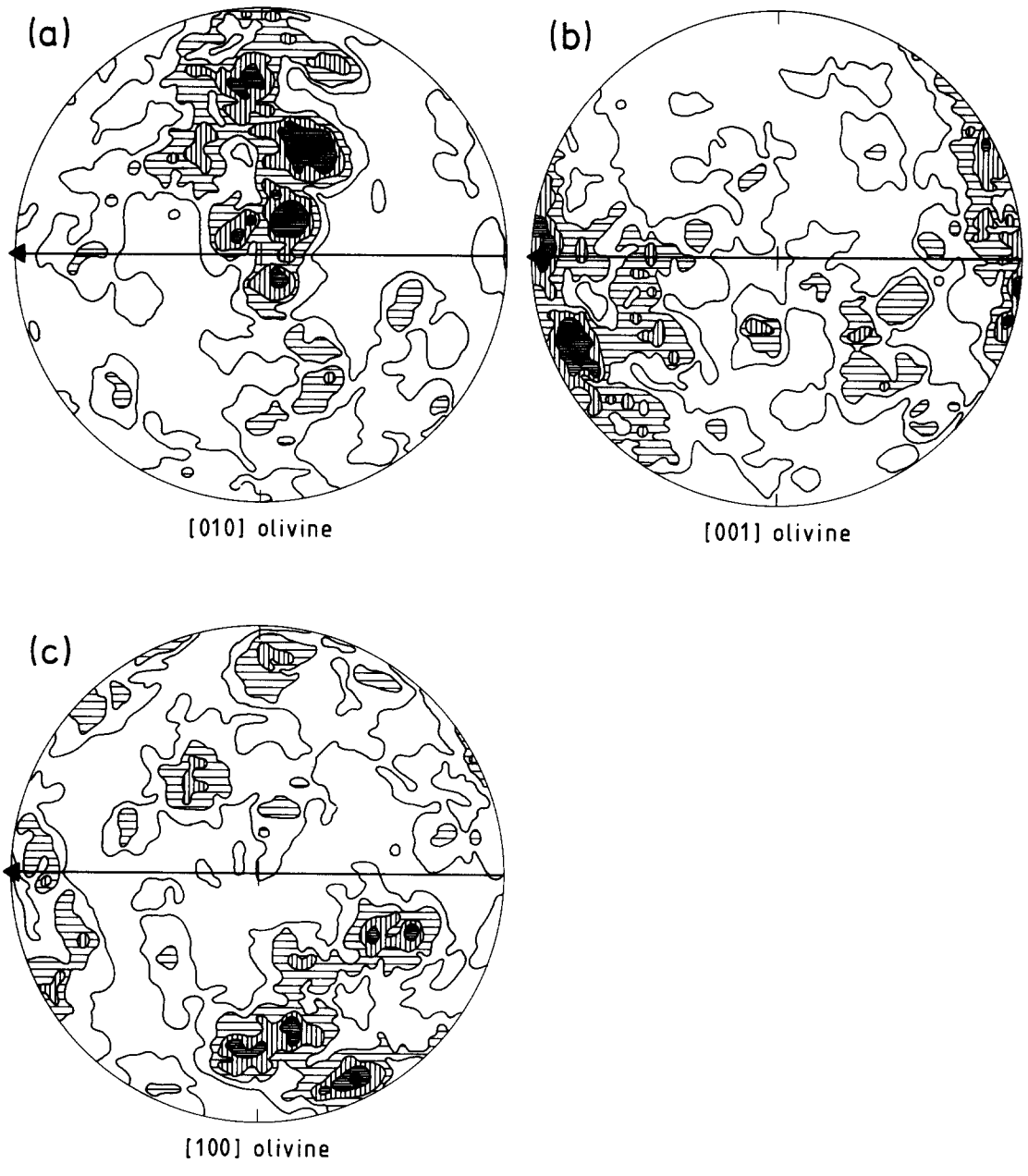

Fig. 6. Deformation texture of dynamically recrystallized olivine (cf. Fig. 4e). Equal-area projections, lower hemisphere, optical measurements on 200 grains. Contours: 1.6–2.4–3.2–4.0–4.8% per 1% area. Trace of foliation = EW, triangle = plunge of stretching lineation. Both are defined by trails of magnetite. Field data: S 300/43, L 280/41. (a) X = [010] olivine, maximum 5.5% (b) Y = [001] olivine, maximum 5.0% (c) Z = [100] olivine, maximum 5.5%.

[100] maximum deviates from the foliation normal by 25° (Fig. 6c).

Activation of an [001] slip direction in olivine can be inferred from [001] lying close to the flow direction L. The slip plane, on the one hand, might have been (100) assuming its obliquity to S to be due to a shear component of flow. On the other hand, the distribution of the [010] main maxima seems to reflect an orientation of {110} close to S splitting up symmetrically. Activation of the {110} [001] and (100) [001] slip systems in olivine can be deduced from these observations.

The common [001] slip direction proves deformation at relatively low temperature (or high-strain rate) (Raleigh 1967, 1968, Carter & Avé Lallemant 1970). This conclusion is supported by the arrangement of subgrain boundaries in recrystallized olivine of a deformation texture. Strained crystals polygonized during recovery forming subgrains about 0.5 mm wide. Two sets of subgrain boundaries developed nearly equally, one parallel to (010) the other parallel to (001). Slip along [010] and [001] is indicated as subgrain boundaries form normal to a preceding slip vector. The (100) [010] slip system operating at the lowest temperature (Raleigh 1967), however, had no visible influence on the [010] texture (Fig. 6a).

Recovery of olivine was part of an annealing history that post-dated dynamic recrystallization after the deformation ceased. It only slightly modified the grain-boundary orientation of the deformation fabric by grain growth. A second generation of metamorphic olivine,

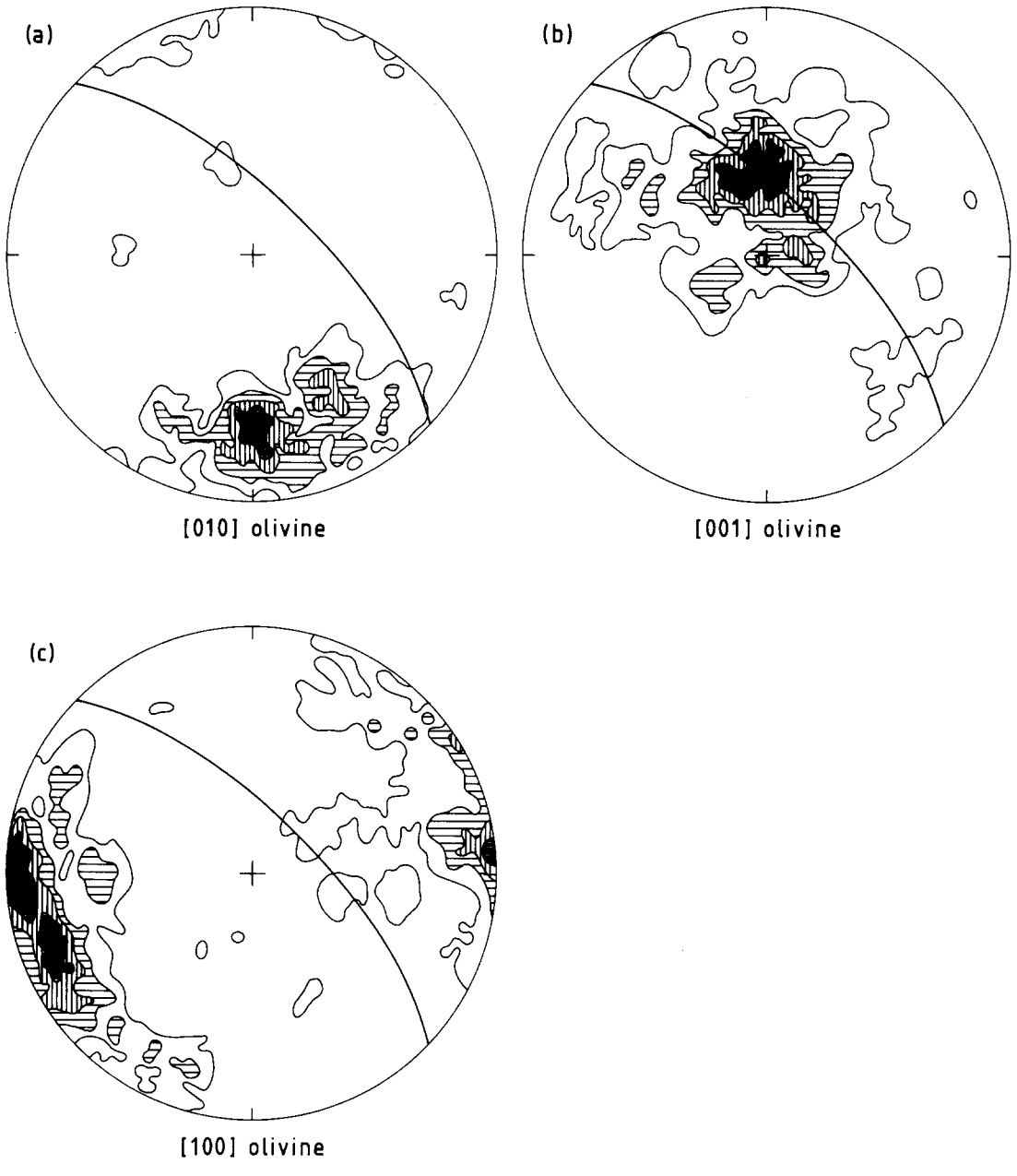

Fig. 7. Texture of recrystallized equigranular fine-grained olivine (cf. Fig. 4h) after static annealing. Equal-area projections, lower hemisphere, optical measurements on 200 grains. Contours: 1.5–3.0–4.5–6.0–7.5% per 1% area. Great circle = weak grain shape foliation. (a) X = [010] olivine, maximum 8.9% (b) Y = [001] olivine, maximum 8.5% (c) Z = [100] olivine, maximum 8%.

however, displays a pure annealing texture. It commonly occurs at grain boundaries of the older generation and at comparable localities of large plastic strain. Contrary to the first generation nearly equant or low axial ratio grains developed, which are small (up to 1 mm) and free of inclusions that commonly cloud the older crystals. Olivine–olivine grain boundaries straightened and equilibrium angles formed at triple junctions (Fig. 4h) due to reduction of grain-boundary energy. Strain-free crystals resulted which exceptionally grew partly idiomorphic after (010). The annealing texture still shows a strong preferred orientation (Fig. 7a–c). A [001] point maximum lies on a weak, broad and partly cleft girdle parallel to the foliation plane, which in this case is a grain shape foliation of olivine as spinel is missing. [010] and [100] both display elongate maxima, [100] nearer to the foliation normal, [010] nearer to the foliation plane. All maxima again split up into two submaxima about 25° apart.

A stretching lineation is hardly visible in the specimen. [001] appears to be the favourable slip direction as it coincides with the foliation plane. The obliquity between [100]/[010] and the foliation points to a {110} slip plane or to slip on (100) if a strong component of shear is presumed. However, no sense of shear can be evaluated as the grain-shape foliation does not define the flow plane exactly. Compared to the deformation texture the high concentrations at the maxima are conspicuous, and the girdles almost vanish. Mercier & Nicolas (1975) suggest large strains to be responsible for stronger concentrations. This agrees well with the occurrence of second generation olivine at high-strain localities. Again

the activation of the [001] slip direction indicates deformation of olivine at relatively low temperatures leading to static annealing. Predominance of the {110} [001] and (100) [001] slip systems strongly contrasts to upper mantle peridotites with an (*okl*) [100] high-temperature slip system dominating (Raleigh & Kirby 1970). Nicolas *et al.* (1980) found (010) [100] slip in olivine within a suboceanic mantle. None of these slip systems were activated here. Consequently no slice of upper mantle was incorporated into this ophiolite fragment, but metacumulates were deformed plastically under crustal conditions.

This deformation obviously took place only along shear zones, leaving large blocks of undeformed cumulates in between. The associated stretching lineation is parallel to the direction of L_1 that formed after serpentinization. As olivine acquired crystallographic preferred orientation and recrystallized, serpentinization could not have happened until later. Afterwards both deformation and annealing textures were replaced by statically grown antigorite (Fig. 4f & g).

An episode of static metamorphism marks the turning point in the subduction–obduction history (Voll 1982). Here it coincides with grain growth of olivine and subsequent static serpentinization. The textural evolution described so far, therefore, should trace back to subduction of the peridotite. Similar fabrics from better preserved peridotites of the Piemonte ophiolite nappe have been ascribed to a subduction process by Fleckenstein & Voll (1982). As will be seen later, one can prove an early obduction history still under conditions of subduction zone metamorphism shortly after serpentinization. For this reason the preceding tectono-metamorphic evolution is probably due to subduction too.

FABRICS OF SERPENTINIZATION

Serpentinization of ultramafic and metamorphic alteration of mafic rocks took place under static conditions resembling those at the termination of fabric development of the peridotite. Within the central part of the layered complex both igneous and metamorphic olivine were replaced by coarse antigorite for the first time. Pseudomorphs mimic the pre-existing fabric. At the margins of the complex, where a strong deformation has obliterated earlier states, the onset of serpentinization remains obscure. Serpentinization from the beginning occurred within the stability field of antigorite (Dietrich & Peters 1971, Trommsdorff 1982). Antigorite commonly occurs in assemblages with diopside, indicating temperatures of low-grade metamorphism (Oterdoom 1978, Trommsdorff & Evans 1974).

Commonly antigorite replacing olivine occurs as irregularly oriented strain-free crystals (Fig. 4b) producing interpenetrating textures (Wicks & Whittaker 1977). Less commonly more equant antigorite formed an interlocking texture especially in the core of pseudomorphs. Hourglass or mesh textures (Wicks *et al.* 1977) cannot be detected even where magnetite still marks the primary fractures of olivine. The absence of mesh rims suggests that chrysotile did not precede antigorite during serpentinization. The average grain size of statically grown antigorite plates is 0.8 × 0.2 mm, grains up to 2.0 × 0.5 mm are common.

Antigorite also replaced clinopyroxene with a more finely grained interlocking texture. A simple pseudomorph may be composed of a few lamellae of different width, and antigorite orientation reflects (100) growth twins of the former pyroxene. When clinopyroxene escaped serpentinization it was sometimes partly replaced by diopside or penninite instead. Orthopyroxene has been completely serpentinized. Except for former orthopyroxene exsolution lamellae in clinopyroxene (Fig. 5d), characteristic pseudomorphs after orthopyroxene are missing—e.g. bastite after kinked enstatite (Wicks 1984). Chromite was altered to magnetite. Replacement started at grain boundaries and cracks, isolating patches of chrome spinel.

Serpentinization of olivine that recrystallized during plastic deformation yielded pseudomorphs easily distinguishable from those developed after magmatic crystals. They are, however, less characteristic as a variety of metamorphic features got lost including grain size, grain shape and grain-boundary texture. Recrystallized olivine has been replaced either by a coarse-grained homogeneous interpenetrating texture or by a more finely grained interlocking texture (Fig. 4g). Again, no mesh textures developed comparable to those found by Wicks (1984) in lizardite pseudomorphs after recrystallized olivine.

DEFORMATIONAL FABRICS AFFECTING THE SERPENTINITE

Deformation after serpentinization resulted in a sequence of events, involving cleavage formation, stretching and folding. Successive events followed the rules of progressive rotational deformation established by Voll (1960) for metapelites in the Scottish Highlands and the Alps (Nabholz & Voll 1963). These events have been numbered D_1–D_4, as D_1 produced the first fabric elements measurable in the field. Deformation did not start everywhere with D_1 and subsequent stages may be missing in places. Where fabrics of magmatic origin are preserved it is obvious that deformation was lacking or weak. The respective sites are inhomogeneously distributed throughout the central complex due to a remarkable inhomogeneous deformation of the serpentinite on the macroscopic scale.

First deformation

During a first step of deformation D_1 a first cleavage S_1 and a first stretching lineation L_1 were produced. S_1 may vary in occurrence from a plane of flattening to a plane of perfect preferred orientation of antigorite basal planes. L_1 is expressed by the disintegration of cumulus spinels into fragment trails, by fibrous magnetite, by the

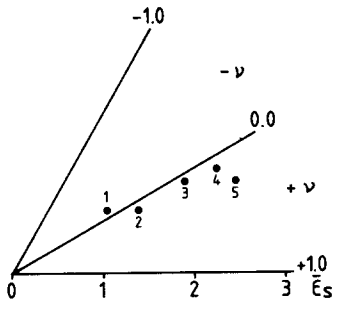

Fig. 8. Hsu-diagram of D_1-strain. Fragment-aggregates of spinel in antigorite schists yield a partial strain of nearly plane strain ($\nu = 0$) symmetry. Points 1 and 4 are from the borders and points 2, 3 and 5 from central parts of the serpentinite. Fifteen measurements per axial ratio of the strain ellipsoid.

long axes of tiny diopside needles and by fibrous growth of antigorite and chlorite especially in tension fractures and pressure shadows.

Inhomogeneity of D_1 applies to both its distribution and intensity. Therefore, the development of S_1 varies from a non-penetrative shear zone deformation to a penetrative schistosity. Strain acquired with D_1 can be measured by the aid of cumulus spinels which were originally equant crystals. Their fragment clusters are flattened in S_1 and stretched parallel to L_1 (Fig. 10). These spinel aggregates yield a strain symmetry $\nu = -0.1$ to $\nu = +0.25$, i.e. a nearly plane strain ($\nu = 0$) for D_1. The strain magnitude ε_s ranges between 1.25 and 2.64. Both are combined in a Hsu-diagram (Fig. 8) following Hossack (1968) and Hsu (1966). Points 1 and 4 come from the margin, points 2, 3 and 5 from central parts of the serpentinite indicating inhomogeneous strain on a macroscopic scale. In general higher strains were reached within shear zones and especially at the western margin where antigorite schists prevail. As cumulus spinels are missing within wide parts of the serpentinite, it is impossible to set up an overall strain profile (cf. Reuber *et al.* 1982). 2.5- to 5.6-fold stretching as well as flattening from 1/2 down to 1/7 of the initial length may thus not be representative of the entire complex. Due to a high ductility contrast only partial strains are derived from spinel deformation.

S_1, where not complicated by younger structures, is relatively flat-lying (Fig. 3b), commonly parallel to the compositional layering (Fig. 3a). This position, however, marks a final stage of deformation. In earlier stages S_1 clearly intersected the layering consistently from top E to bottom W, i.e. first folds are missing. The intersection line β_1 of layering and S_1 plunges NNW (Fig. 3b).

In several places the development of S_1 and L_1 during progressive rotational deformation can be studied almost from the beginning of D_1. Where igneous layering is marked by clinopyroxenites they can be used like sedimentary bedding in common structural analysis. The pyroxenes decomposed to penninite–diopside aggregates embedded in a groundmass of antigorite both lacking any preferred orientation. The neighbouring serpentinites display an interpenetrating texture.

S_1 started as a conjugate system of shear planes with differing sense of displacement. According to Voll (1960, p. 554) one may call the narrowly spaced set antithetic S_{1a}, and the more widely spaced synthetic S_{1s}; these terms relate the displacement to the total rotation due to deformation (Hoeppener 1955). The sense of total rotation during D_1 was directed ESE.

Progressive rotational deformation resulted in: (1) progressive synthetic rotation of both S_{1s} and S_{1a}; (2) decrease of the angle between S_{1s} and S_{1a} as well as decrease of angular spread within each set; and (3) reduction of width between the shear planes. This evolution is shown in Fig. 3(c) for five stages. The angle between S_{1s} and S_{1a} diminishes from 44° over 34°, 15° and 10° down to 5°. There, S_1 appears macroscopically penetrative. The width between S_{1s} planes at the same time decreases from 9 to 5 mm, over 2–5 mm, to smaller than 2 mm. Contemporaneously S_1 lost its anastomosing habit and a first slaty cleavage developed at the end (Williams 1979). Lines of S_{1s}/S_{1a}-intersection β_1 gently plunge N (Fig. 3c). The first stretching lineation L_1 is rarely evident in the beginning of D_1. L_1 makes its appearance on S_{1s} first, plunging constantly WNW–ESE even after a strong first deformation (Fig. 3b).

D_1 *deformation mechanisms*

As serpentinization preceded deformation the high strength of pseudomorphic serpentinite had to be overcome during its transformation into antigorite schists. Raleigh & Paterson (1965) expected a brittle–ductile transitional behaviour under low-grade metamorphic conditions. These authors and Dengo & Logan (1981) emphasize that serpentinites of different texture and mineralogical composition cannot be regarded as mechanically equivalent. From microscopic observations in the Gouffre serpentinite it is obvious that various deformation mechanisms became effective during D_1.

Fracturing is commonly observed in interpenetrating and interlocking textures. Shear fractures allow fragments to rotate individually. Tension fractures open between and pressure shadows abut upon fragments. Both were filled by newly grown platy antigorite with its long axis parallel to L_1. The void-filling antigorite also replaced marginal parts of the pseudomorphic texture (Fig. 5a) close to σ_3. Such replacement did not occur at boundaries adjacent to σ_1. There is a sharp contact between the interpenetrating texture and antigorites lying strictly parallel S_1 exists (Fig. 5a). The interpenerating antigorites at these margins were not bent or kinked even where they meet them under high angles. The boundary surface appears microscopically stepped with steps tied to grain boundaries of the pseudomorphic texture. Fine-grained magnetite is sometimes enriched there. These features indicate pressure solution of pseudomorphous antigorite as a further deformation mechanism, serving as a source of antigorite redeposited in opening voids.

Though evidence of plastic deformation is rare within interpenetrating textures, it is commonly found within bastites. Polygonization of bent bastites led to the forma-

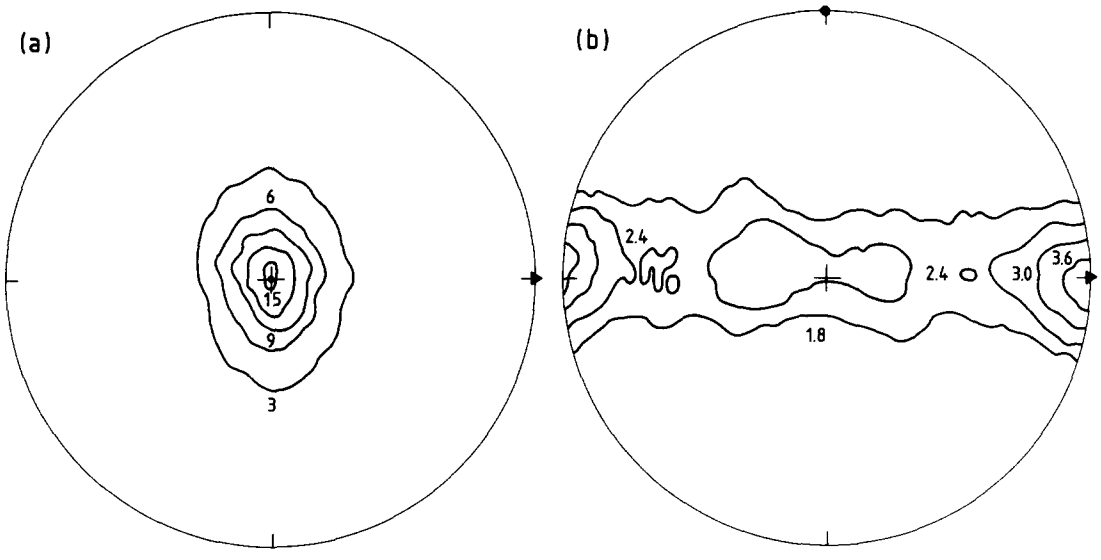

Fig. 9. X-ray fabric diagrams for antigorite from antigorite schist. Combined reflection scans measured on three mutually perpendicular slabs. Plane-strain deformation $\nu = -0.1$, $\varepsilon_s = 1.23$. The full circle denotes the pole of the penetrative first cleavage, the triangle marks L_1. (a) Antigorite (001) pole figure, the normal to S_1 in the centre, L_1 EW. (b) Antigorite [010] texture with S_1 and L_1 EW. Contours in multiples of an uniform distribution. Equal-area, lower hemisphere.

tion of subgrains with subgrain boundaries partly euhedral after (001) and strongly serrated parallel to (010) (Fig. 5b). A low-angle misfit up to 6° for all three crystallographic axes may exist between neighbouring subgrains. The subgrain size decreased with stronger deformation from 0.2 × 0.05 mm to 0.05 × 0.01 mm, measured parallel and normal to (001).

Recrystallization started at subgrain boundaries (Fig. 5b), kink-band boundaries, or even at basal planes after imperfect slip due to strong bending of antigorite (Fig. 5e). A special orientation relationship between recrystallized grains and the parent grain is comparable to cross-micas (Sander 1930, p. 215). Cross-antigorites preferentially grew with a high angular deflection of (001) from the parent grain, angles of 60 and 90° clearly predominate (Fig. 5e). Recrystallization thus rapidly replaced the deformed volume of serpentinite. Since most of the plastically deformed bastites were oriented with (001) near to the principal compressive stress, resulting cross-antigorites acquired an attitude suitable for basal glide. Thus, growth of cross-antigorite may involve a weakening effect.

However, the role of crystallographic slip combined with mechanical rotation during the development of antigorite schists has not yet been proven. The only argument supporting the activation of this deformation mechanism so far has been the strong planar preferred orientation of (001) parallel to the schistosity. Such (001)-texture is shown on Fig. 9(a) derived from an antigorite schist measured with an X-ray texture goniometer. In addition to the planar fabric a remarkable linear fabric also exists. The [010]-texture of antigorite (Fig. 9b) forms a girdle in S_1 with a strong maximum of [010] at L_1. Two poorly defined submaxima nearly 20° inclined to the normal to L_1 also occur. The girdle tends to disappear at the expense of the main maximum. This preferred orientation is found in the plane strain environment indicated by spinel deformation with $\nu = 0.1$ and $\varepsilon_s = 1.23$ (point 1 in Fig. 8). It suggests the predominance of an (001) [010] slip system for antigorite. [010] is the only basal slip direction not conflicting with the polarity reversals (Kunze 1956) of the curved antigorite layers. However, as this slip system alone was not able to produce the observed fabric from a random distribution one still has to assume the contribution of dynamic recrystallization. Crystals of antigorite oriented parallel to S_1 are smaller than those in statically grown pseudomorphs; they are generally about 0.3 × 0.04 mm but cover the whole range of subgrain size mentioned above. The shape anisotropy is more pronounced, length to width ratios rising to 10.

Second deformation

Second folds, B_2, folded the first cleavage for the first time (Fig. 3d) with axes strictly parallel to L_1 (Fig. 3e). They occur only in places with a strong preceding D_1-deformation, e.g. near the margins of the complex and at boundaries between the different lithological units, especially near the contact of serpentinite–metagabbro against metasedimentary rocks (Fig. 2). There, wavelength and amplitudes of B_2 reach several tens of metres, folding the metasediments deeply into the serpentinite. Within the central serpentinite B_2 folds are smaller; they reach dm- to m-scale. Isoclinal to tight folds prevail; interlimb angles very rarely reach 90°. Their hinges are rounded and second-order B_2 folds occur especially on their short limbs. Intrafolial folds are found in competent layers as metagabbros, pyroxenites and rodingite dykes in a matrix of serpentinite. The vergence of B_2 folds is commonly directed SW; NE-vergence also occurs, both frequently combined in polyvergent folds (Fig. 10). Axial planes of B_2 folds build up a convergent fan. S_2 forms an axial plane foliation (Fig. 3e). It may be a

crenulation type or even be missing in more competent layers. Where D_2 was strong, a second stretching lineation L_2 developed. Again it is marked by fibrous antigorite, chlorite and magnetite now growing on S_2. L_2 plunges WNW–ESE as L_1 did previously (Fig. 3e).

Second folds are of special importance since they structurally linked the serpentinite to the metasedimentary rocks. That is, a single B_2 fold simultaneously folded both serpentinite and metasediments and their contact surface. Thus B_2 folds prove a common tectonometamorphic history of both units, at least since the beginning of D_2. The conditions of metamorphism, however, can be evaluated in the metasediments much more precisely. The metasedimentary rocks belong to the Garten-Rifelberg formation (Bearth 1967, Dal Piaz & Ernst 1978). They have passed an early-Alpine (Cretaceous) stage of subduction zone metamorphism (eclogites, quartz–garnet–omphacite–glaucophane–zoisite –phengite–schists), followed by decompression and tectonic rise (glaucophanic blueschists), succeeded by greenschist-facies assemblages (with actinolitic amphibole–chlorite–biotite–epidote and albite). Fabric development during D_1 and D_2 in the metasediments joining the serpentinite is correlated with the high-pressure subduction zone metamorphism. Jadeitic pyroxene and glaucophane did grow along S_1, were bent around B_2 and afterwards healed without changing composition. Ernst & Dal Piaz (1978) evaluated $T = 470 \pm 50$°C and $P = 10 \pm 2$ kb for subduction zone metamorphism in this unit. The same conditions consistently apply to the serpentinite during D_2. Within the serpentinite antigorite bent round B_2 recrystallized, forming polygonal arcs. A grain size similar to D_1 was achieved. Diopside and forsterite remained stable beside antigorite during D_2 and both minerals recrystallized after B_2 folding.

Third deformation

Third folds folded S_2 for the first time, S_1 for the second time. As they are nearly homogeneously distributed throughout the serpentinite one finds them frequently where B_2 folds are missing. There, B_3 folds folded S_1 (Fig. 3f) or even the igneous layering (serpentinized) for the first time (Fig. 3a). Third folds are angular kinks with a pronounced monoclinic symmetry. Usually wavelength and amplitudes reach some dm or m. Vergence is directed E for first-order B_3 folds. Second-order B_3 folds change vergence from E on long limbs to W on short limbs of first-order B_3 folds. Westward vergence on a regional scale is found within the short limb of a B_3 mega-kink, about 100 m thick and running N–S through the Western serpentinite (Fig. 2). Its hinges are marked by second-order B_3 folds of nearly orthorhombic symmetry (chevron folds).

Axes of B_3 folds and lines of S_3/S_1-intersection β_3 plunge subhorizontally, the directions of plunge being widely scattered around N–S. Scatter of data is partly due to curving B_3 axes. The plunge of a single axis may repeatedly turn through 25° in different directions (Fig. 3g), not necessarily lying within an axial plane. There is no correlation between the various plunge directions and different interlimb angles (Grocott & Watterson 1980) of 24–120° usually reaching 40–80°.

The strong planar anisotropy of S_1 gave rise to a widely spaced third crenulation cleavage, S_3 (Figs. 5c and 10). S_3 developed as a conjugate system, as S_1 did in the beginning. A synthetic set, S_{3s}, yielded slip supporting total rotation, an antithetic set, S_{3a}, worked against it at the same time (Fig. 5c). As found in phyllites (Hoeppener 1956) both rotated synthetically with progressive deformation. Beginning with a steep attitude the angle of dip successively diminished finally leading to a gently W-dipping S_3 (Fig. 3g). S_{3s} preceded S_{3a} during rotation in the sense of total rotation (Voll 1960, p. 554), i.e. eastward for D_3 (Fig. 3h). Both sets are frequently inclined to one another by as much as 15–25°. Spacing of S_3 varies between several cm down to some mm. Folds connected with S_3 show a characteristic distribution of S_3 in the beginning. S_3 as a whole forms a convergent fan, but S_{3a} and S_{3s} are restricted to the long and short limb of B_3, respectively (Fig. 10). Both sets of S_3 may join one another in the hinge region. With progressive folding S_{3a} and S_{3s} occur on both limbs of B_3 together. An L_3 stretching lineation only formed on S_{3s} if this approached mm-spacing. Fibrous magnetite and antigorite indicates L_3 plunging WNW (Fig. 3g) as L_1 and L_2 did previously.

Antigorites bent round B_3 recrystallized only where large strains were imposed. There, very small (0.07 × 0.03 mm) cross-antigorites grew at the expense of strained crystals. The conspicuous decrease in grain size and the small volume recrystallized suggest decreasing temperature. However, diopside still was stable beside antigorite. Fine-grained diopside formed polygonal arcs round B_3 folds, while larger crystals of an older generation were broken during D_3.

Fourth deformation

D_4 shows a very inhomogeneous, spotted distribution. Even where D_3 had proceeded considerably, D_4 did not necessarily develop. Structures of D_4, however, indicate an origin due to progressive deformation. The rotational component of the preceding events was maintained during D_4.

S_4 occurred with an antithetic set of cleavage planes first, where the angle between S_{3a} and S_{3s} shrunk below 25°, i.e. where S_3 approached an orientation nearly perpendicular to the axis of maximum shortening. S_{4a} intersects S_1 at a high angle steeply dipping WNW or ESE (Fig. 3i) as S_3 did during early stages of D_3 (Fig. 3g). A typical arrangement of the D_3–D_4 succession round a B_3 fold is shown on Fig. 3(k), the acute angle between S_{3a} and S_{3s} including the direction of maximum extension. S_{4a}, although slightly deflected, nearly lies in a plane of maximum shear of the D_3 strain ellipsoid. It is found on long limbs of B_3 folds, where S_{4a} displays a dm- to cm-spacing rarely evolving to a mm-spaced crenulation cleavage.

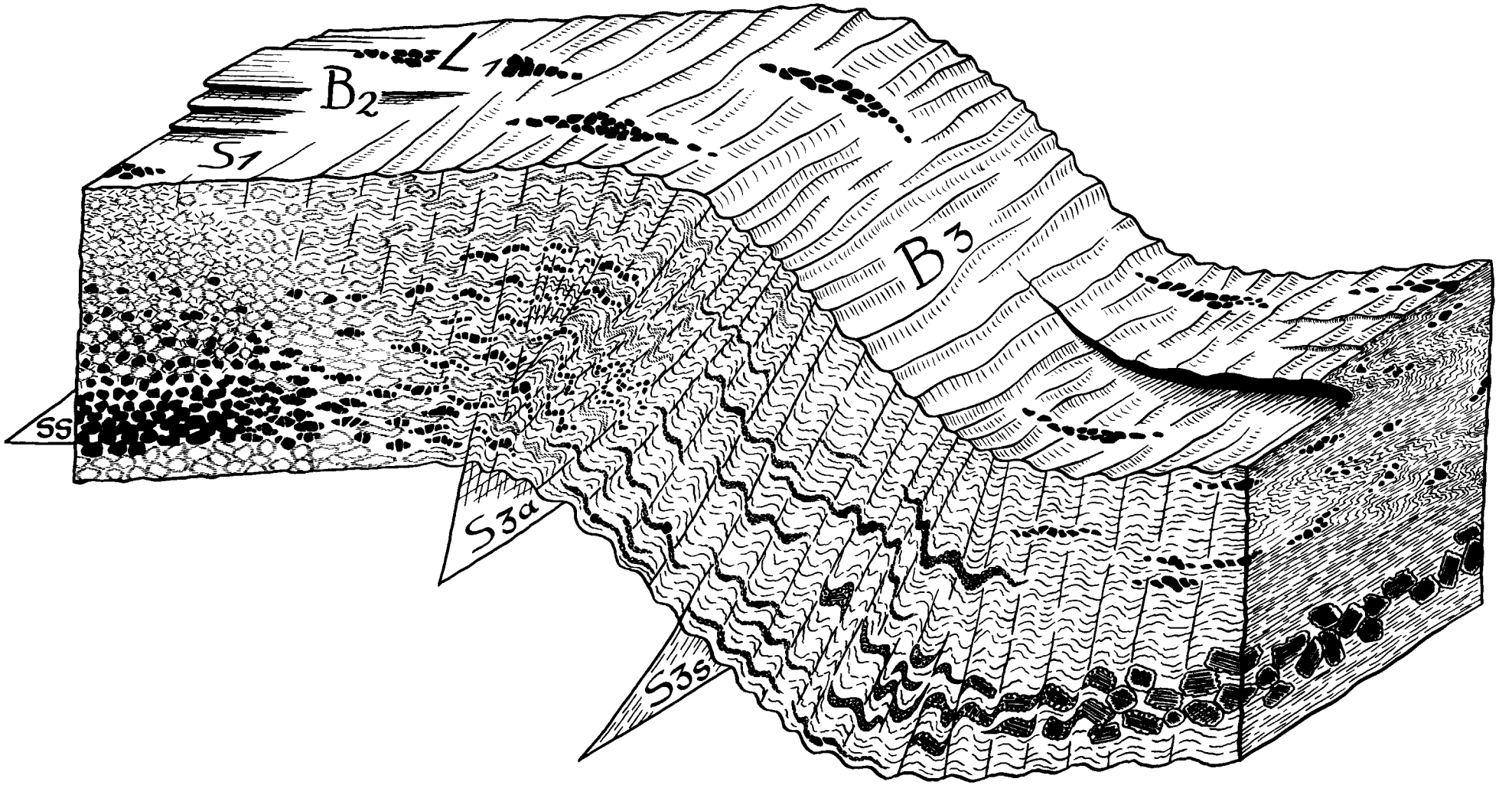

Fig. 10. Structural details from the Gouffre serpentinite. Looking north magmatic and tectonic fabrics are shown within the frame of an E-vergent third fold of 1 m length. On the left a pseudomorphic cumulus fabric combines igneous layering (*SS*) with grain size plus modal grading upwards of chromite and olivine. On the right is clinopyroxenite. D_1 increases toward the central part of the drawing: light antigorite pseudomorphs vanish into schistose serpentinite with S_1-flattening and L_1-stretching. Magnetite pseudomorphs after chrome spinel underwent brittle deformation first. Later with D_1 their fragment aggregates were replaced by fibrous magnetite. Clinopyroxene became pseudomorphed only where strong D_1-strains were imposed. Polyvergent B_2 folds have axes parallel to L_1. Third folds B_3 emerge as large kinks folding *SS*, S_1, L_1 and B_2 combined with a third crenulation cleavage S_3. S_3 splits into an antithetic S_{3a} working against D_3 total rotation and restricted to the long limb and a synthetic S_{3s} supporting total rotation on the short limb. A third stretching lineation may occur on S_{3s} trending parallel to L_1.

Fourth folds, B_4, commonly stay small and very open. Only exceptionally D_4 produced open monoclinic folds in the m-range with interlimb angles reaching 160–130°. B_4 folds verge ESE. Axes of B_4 folds and the S_4–S_1 intersection lines mainly plunge SSW (Fig. 3i). Thus, B_4 may fold B_3 despite their partly similar distribution. A fourth stretching lineation is not present.

The youngest structures refer to the subnappe boundary at the SE margin of the Gouffre serpentinite (Fig. 2). There, deformation is dominated by brittle mechanisms leading to a considerable grain size reduction. Cataclastic fault rocks evolved with a pronounced NW–SE stretching lineation. This in turn induced remarkable folding with axes parallel to the stretching lineation. Mineral assemblages and textures indicate a low-grade metamorphism outlasting even this deformation, probably of late-Alpine age. Work, however, is still in progress.

DISCUSSION AND CONCLUSIONS

Fabric development in the Gouffre serpentinite has been presented in relative chronological order. Now we shall try to fit the observations into a plate tectonic model adopted for the Western Alps (Dal Piaz *et al.* 1972, Laubscher 1975, Frisch 1979, Beccaluva *et al.* 1984).

Formation of the protolith traces back to igneous activity at the spreading ridge of the Jurassic Piemonte Ocean. Thick cumulate peridotites overlain by cumulate gabbros contribute to the oceanic crust. These observations contrast to some degree with a genetic model for the Western Alpine ophiolites (Lombardo & Pognante 1982) favouring ultramafic tectonites as the basal layer instead of ultramafic cumulates. Upper mantle tectonites, however, are completely missing in this ophiolite fragment. Igneous layering is prominent and still has an upright position judging from density stratification. Current bedding in the mafic unit indicates a magma flow directed NW. Assuming the magma flow to result from thermal convection in the magma chamber, currents should have been directed downslope above the accumulating bottom layer (Wager & Brown 1968). Bottom layers gently inclined to the ridge follow from a bilateral magma chamber with a funnel shaped cross-section (Cann 1974, Pallister & Hopson 1981). Adopting such a model one might expect the Piemonte spreading axis relatively further NW, inferred from dip of layering, trough structure and current directions. The complex tectonic history of the Piemonte ophiolite nappe may have altered the dip and plunge of primary structures. It could not, however, have changed the fossilized current directions. As this conclusion is the very first attempt to reconstruct the regional provenance of Piemonte oceanic crust, one still has to proceed with caution.

Sea floor spreading has not been documented in the Gouffre peridotite, neither as a deformational event nor as an ocean floor metamorphism (Miyashiro *et al.* 1971, Weissert & Bernoulli 1985). However, deformation started under brittle conditions for cumulus olivine combined with a crack–seal mechanism (Ramsay 1980). As both these processes are characteristic of a crustal environment (Ashby & Verrall 1977, Ramsay 1980), one has to assume considerable cooling of the cumulates from the peridotite solidus temperature (about 1150°C, Ito & Kennedy 1967) down to low-grade metamorphic conditions. Such cooling due to conduction requires a significant period of time (Kusznir 1980).

The next step of deformation introduced plastic deformation of olivine. This is important as it reveals 2-fold information: firstly the ultramafics cannot have been serpentinized until then, and secondly the changing deformation mechanism indicates prograde metamorphism during olivine deformation. Prograde metamorphism corresponded to subduction as the serpentinite shared subduction zone metamorphism during its tectonic rise (D_2). This implies earlier subduction of the metaperidotite. The transitional depth from fracturing to plastic deformation of olivine (35 km, Ashby & Verrall 1977) may rise with decelerating strain rate, while depression of isotherms during subduction (Toksöz *et al.* 1971) yields an opposite effect.

Deformation during subduction occurred along shear zones leaving undeformed cumulates in between. Plastic flow on shear zones was achieved by dislocation glide in olivine. The (100) [010], (100) [001] and {110} [001] slip systems have been activated, judging from subgrain boundaries and textures with [001] subparallel to an early spinel lineation. Referring to Raleigh (1967, 1968) and Phakey *et al.* (1972) these slip systems operate at relatively low temperature (or high-strain rate). Their activation has never been observed in upper mantle peridotites (Mercier & Nicolas 1975). Even where harzburgite tectonites constitute the uppermost mantle beneath ophiolite cumulates they have been deformed by high-temperature slip of olivine with a [100] slip direction (Nicolas *et al.* 1980, Ozawa 1983). Consequently no slices of upper mantle contributed to the Gouffre serpentinite, either due to mantle upwelling or as tectonic wedges. Little is known about the transitional temperature from [001] to [100] slip in olivine at natural conditions. Nicolas *et al.* (1980) suggest it to be higher than 500°C and Kruhl & Voll (1979) place it at the amphibolite–granulite-facies boundary, i.e. near 600°C. According to Voll (1985) olivine recrystallizes down to 450°C giving a lower limit of the temperature span during plastic flow. The pressure dependence of the slip system activated (Carter & Avé Lallemant 1970) as well as the weakening effect of P_{H_2O} (Blacic 1971) are negligible here. Pressure greater than 10 kb may be inferred from the steep geothermal gradient of 9–15°C km^{-1} found in the ophiolite nappe (Chinner & Dixon 1973, Meyer 1983). The next step in fabric development was one of static annealing post-dating dynamic recrystallization. Recovery led to polygonization of strained olivine and grain growth affected especially smaller crystals of a second generation producing polygonal shaped grains. Annealing fabrics indicate a pause in deformation that

has been found to mark the turning point from subduction to obduction within several subducted Alpine rock series (Richter & Voll 1982, Voll 1982, Vogler 1984). At this turning point the uppermost parts of the downgoing lithosphere must have decoupled from continuing subduction. Welded to the hanging wall they remained fixed at conditions of subduction zone metamorphism lacking any subsequent deformation. Applied to the Piemonte ophiolite case old oceanic crust remained fixed to the southern plate, while after progradation to the NW (Roeder 1976) continuing subduction pulled down the underlying mantle and later on younger oceanic crust (Nicolas & Le Pichon 1980). The entire Piemonte basin must have passed that way and both continental margins have been subducted too (Compagnoni *et al.* 1977, Chopin & Monié 1984). Dehydration of younger oceanic crust and sediments during metamorphism possibly gave rise to the fluids penetrating the ophiolite segment coupled to the cover plate, thus changing its peridotites into antigorite serpentinites. Therefore, static metamorphism marked both the last event of fabric development in the peridotite and the beginning of serpentinization. From this it is concluded that serpentinization occurred also at the turning point prior to obduction. Resulting coarse-grained pseudomorphous antigorite serpentinite survived in many places due to its high mechanical strength.

Deformation of the serpentinite was a result of a progressive rotational deformation. Total rotation (Hoeppener 1956) to the SE was maintained during successive events D_1–D_4. This is important as the rotational component of deformation here was induced by friction at the rigid hangingwall dipping SE. From that a different sense of total rotation has to result, directed NW during subduction and SE during obduction. Deformation of the serpentinite, therefore, referred to obduction alone. It was a tectonic event more than a buoyant rise (England & Holland 1979). At that time the Gouffre serpentinite was part of the cover plate that possibly emerged under compression forming deep reaching accretionary wedges. D_1 started with a conjugate system of shear planes in a plane-strain environment. Antigorite shows pressure solution, fracturing and crystallographic slip on (001) [010] accompanying recrystallization. The operation of three deformation mechanisms for one mineral species at the same time seems to contradict their dependence on stress and temperature (Ashby 1972). One reason for that may be the different mechanical behaviour of different antigorite textures.

D_2 produced folds with axes parallel to the stretching lineation L_1. These folds are important as they structurally linked the serpentinite to metasedimentary rocks, proving a common tectono-metamorphic history of both units at least since that stage. The metasediments prove high-pressure subduction zone metamorphism during D_2. Jadeitic pyroxene and glaucophane remained stable and Ernst & Dal Piaz (1978) evaluated $T = 470 \pm 50$°C and $P = 10 \pm 2$ Kb for this unit. Combining this metamorphic argument with the structural one favoring obduction, D_1 as well as the static serpentinization must have been part of even deeper subduction. As the structural evolution of the Gouffre serpentinite was a continuous process, D_1–D_4 deformation was probably entirely of early-Alpine age (Hunziker 1974). The Oligocene continental collision may only be responsible for the subnappe structures and concomitant low-grade metamorphism in this part of the Western Alps.

Acknowledgements—Support from the Deutsche Forschungsgemeinschaft grant Vo 92/16 is gratefully acknowledged. I thank Dr B. Stöckhert and three anonymous referees for their thoughtful comments that substantially improved the manuscript. Special thanks are also due to Dr J. P. Platt for his detailed editorial comments.

REFERENCES

Ashby, M. F. 1972. A first report on deformation-mechanism maps. *Acta Metall.* **20**, 887–897.

Ashby, M. F. & Verrall, R. A. 1977. Micromechanisms of flow and fracture, and their relevance to the rheology of the upper mantle. *Phil. Trans. R. Soc. Lond.* **A288**, 59–95.

Bearth, P. 1967. Die Ophiolithe der Zone von Zermatt-Saas Fee. *Beitrag geol. Karte Schweiz, N.F.* **132**, 130.

Beccaluva, L., Dal Piaz, G. V. & Macciotta, G. 1984. Transitional to normal MORB affinities in ophiolitic metabasites from the Zermatt–Saas, Combin and Antrona units, Western Alps: implications for the paleogeographic evolution of the Western Tethyan Basin. *Geologie Mijnb.* **63**, 165–177.

Blacic, J. 1971. Hydrolytic weakening of quartz and olivine. Unpublished Ph.D. thesis, University of California, Los Angeles.

Cann, J. R. 1974. A model for oceanic crustal structure developed. *Geophys. J. R. astr. Soc.* **39**, 169–187.

Carter, N. L. & Avé Lallemant, H. G. 1970. High temperature flow of dunite and peridotite. *Bull. geol. Soc. Am.* **81**, 2181–2202.

Chinner, G. A. & Dixon, J. E. 1973. Some high-pressure parageneses of the Allalin Gabbro, Valais, Switzerland. *J. Petrol.* **14**, 185–202.

Chopin, C. 1981. Talc-phengite: a widespread assemblage in high-grade pelitic blueschists of the western Alps. *J. Petrol.* **22**, 628–650.

Chopin, C. & Monié, P. 1984. A unique magnesiochloritoid-bearing, high-pressure assemblage from the Monte Rosa, Western Alps: petrologic and ^{40}Ar–^{39}Ar radiometric study. *Contr. Miner. Petrol.* **87**, 388–398.

Coleman, R. G. 1977. *Ophiolites: Ancient Oceanic Lithosphere?* Springer Verlag, Berlin.

Compagnoni, R., Dal Piaz, G. V., Hunziker, J. C., Gosso, G., Lombardo, B. & Williams, P. F. 1977. The Sesia–Lanzo Zone, a slice of continental crust with alpine high pressure–low temperature assemblages in the western Italian Alps. *Rc. Soc. ital. miner. Petrol.* **33**, 281–334.

Dal Piaz, G. V. 1974. Le metamorphisme de haute pression et basse temperature dans l'evolution structurale du bassin ophiolitique alpino-apenninique. *Schweiz. miner. petrogr. Mitt.* **54**, 399–424.

Dal Piaz, G. V., Hunziker, J. C. & Martinotti, G. 1972. La zona Sesia-Lanzo e l'evoluzione tettonico-metamorfica delle Alpi Nordoccidentali interne. *Mem. Soc. geol. ital.* **11**, 433–460.

Dal Piaz, G. V. & Ernst, W. G. 1978. Areal geology and petrology of eclogites and associated metabasites of the Piemonte Ophiolite Nappe, Breuil–St. Jacques area, Italian Western Alps. *Tectonophysics* **51**, 99–126.

Dengo, C. A. & Logan, J. M. 1981. Implications of the mechanical and frictional behavior of serpentinite to seismogenic faulting. *J. geophys. Res.* **86**, 10771–10782.

Dietrich, V. M. & Peters, T. 1971. Regionale Verteilung der Mg-Phyllosilikate in den Serpentiniten des Oberhalbstein. *Schweiz. miner. petrogr. Mitt.* **51**, 329–348.

England, P. C. & Holland, T. J. B. 1979. Archimedes and the Tauern eclogites: the role of buoyancy in the preservation of exotic eclogite blocks. *Earth Planet. Sci. Lett.* **44**, 287–294.

Ernst, W. G. & Dal Piaz, G. V. 1978. Mineral parageneses of eclogitic rocks and related mafic schists of the Piemonte ophiolite nappe, Breuil-St. Jacques area, Italian Western Alps. *Am. Miner.* **63**, 621–640.

Fleckenstein, M. & Voll, G. 1982. Die Geschichte subduzierter Peridotite in der Piemonteser Zone der Westalpen. *Fortschr. Miner.* **60**, 74–76.

Frisch, W. 1979. Tectonic progradation and plate tectonic evolution of the Alps. *Tectonophysics* **60**, 121–139.

George, R. P., Jr. 1978. Structural petrology of the Olympus ultramafic complex in the Troodos ophiolite, Cyprus. *Bull. geol. Soc. Am.* **89**, 845–865.

Gosso, G., Dal Piaz, G. V., Piovano, V. & Polino, R. 1979. High pressure emplacement of early-Alpine nappes postnappe deformations and structural levels (Internal Northwestern Alps). *Memorie Ist. geol. miner. Univ. Padova* **32**, 1–15.

Gosso, G. & Messiga, B. 1977. Promindo: analisi strutturale di un complesso di calcescisti s.l. e metabasiti. In: *Escursione ad alcuni giacimenti a Cu–Fe e Mn della falda Piemontese, Alpi occidentali*, 10–13 Ottobre 1977. *Ofioliti* **2**, 256–258.

Grocott, J. & Watterson, J. 1980. Strain profile of a boundary within a large ductile shear zone. *J. Struct. Geol.* **2**, 111–117.

Hoeppener, R. 1956. Zum Problem der Bruchbildung, Schieferung und Faltung. *Geol. Rdsch.* **45**, 247–283.

Hossack, J. R. 1968. Pebble deformation and thrusting in the Bygdin area (Southern Norway). *Tectonophysics* **5**, 315–339.

Hsu, T. C. 1966. The characteristics of coaxial and non-coaxial strain paths. *J. Strain Anal.* **1**, 216–222.

Hunziker, J. C. 1974. Rb–Sr and K–Ar age determination and the Alpine tectonic history of the Western Alps. *Memorie Ist. geol. miner. Univ. Padova* **31**, 54.

Irvine, T. N. 1975. Crystallization sequences in the Muscox intrusion and other layered intrusions—II. Origin of chromitite layers and similar deposits of other magmatic ores. *Geochim. cosmochim. Acta* **39**, 991–1020.

Ito, K. & Kennedy, G. C. 1967. Melting and phase relations in a natural peridotite to 40 kilobars. *Am. J. Sci.* **265**, 519–538.

Jackson, E. D. 1967. Ultramafic cumulates in the Stillwater, Great Dyke and Bushveld intrusions. In: *Ultramafic and Related Rocks* (edited by Wyllie, P. J.). Wiley, New York, 20–38.

Jackson, E. D., Green II, H. W. & Moores, E. M. 1975. The Vourinos Ophiolite, Greece: cyclic units of lineated cumulates overlying harzburgite tectonite. *Bull. geol. Soc. Am.* **86**, 390–398.

Jacques, A. L. 1981. Petrology and petrogenesis of cumulate peridotites and gabbros from the Marum ophiolite complex, Northern Papua New Guinea. *J. Petrol.* **22**, 1–40.

Kruhl, J. H. & Voll, G. 1979. Deformation and metamorphism of the western Finero complex. *Memorie Ist. geol. miner. Univ. Padova* **33**, 95–109.

Kunze, G. 1956. Die gewellte Struktur des Antigorits, I. *Z. Kristallogr.* **108**, 82–107.

Kusznir, N. J. 1980. Thermal evolution of the oceanic crust; its dependence on spreading rate and effect on crustal structure. *Geophys. J. R. astr. Soc.* **61**, 167–181.

Laubscher, H. P. 1975. Plate boundaries and microplates in Alpine history. *Am. J. Sci.* **275**, 865–876.

Lombardo, B. & Pognante, U. 1982. Tectonic implications in the evolution of the Western Alps Ophiolite metagabbros. *Ofioliti* **7**, 371–394.

Mattirolo, E. 1912. Fo. 29 Monte Rosa. Carta Geol. d'Italia 1:100.000. *Boll. R. Uff. geol. Ital. Roma.*

Mercier, J.-C. D. & Nicolas, A. 1975. Textures and fabrics of upper-mantle peridotites as illustrated by xenoliths from basalts. *J. Petrol.* **16**, 454–487.

Meyer, J. 1983. The development of the high-pressure metamorphism in the Allalin metagabbro (Switzerland). *Terra cognita* **3**, 187.

Miyashiro, A., Shido, F. & Ewing, M. 1971. Metamorphism in the Mid-Atlantic Ridge near 24° and 30° N. *Phil. Trans. R. Soc. Lond.* **A268**, 589–603.

Moores, E. M. & Vine, F. 1971. The Troodos massif, Cyprus and other ophiolites as oceanic crust: evaluation and complications. *Phil. Trans. R. Soc. Lond.* **A268**, 443–466.

Nabholz, W. K. & Voll, G. 1963. Bau und Bewegung im gotthard-massivischen Mesozoikum bei Ilanz (Graubünden). *Eclog. geol. Helv.* **56**, 755–808.

Nicolas, A., Boudier, F. & Bouchez, J.-L. 1980. Interpretation of peridotite structures from ophiolitic and oceanic environments. *Am. J. Sci.* **280**, 192–210.

Nicolas, A. & Le Pichon, X. 1980. Thrusting of young lithosphere in subduction zones with special reference to structures in ophiolitic peridotites. *Earth Planet. Sci. Lett.* **46**, 397–406.

Oterdoom, W. H. 1978. Tremolite- and diopside-bearing serpentine assemblages in the CaO–MgO–SiO_2–H_2O multisystems. *Schweiz. miner. petrogr. Mitt.* **58**, 127–138.

Ozawa, K. 1983. Relationships between tectonite and cumulate in ophiolites: the Miyamori ultramafic complex, Kitukami Mountains, Northeast Japan. *Lithos* **16**, 1–16.

Pallister, J. S. & Hopson, C. A. 1981. Samail ophiolite plutonic suite: field relations, phase variation, cryptic variation and layering, and a model of a spreading ridge magma chamber. *J. geophys. Res.* **86**, 2593–2644.

Phakey, P., Dollinger, G. & Christie, J. M. 1972. Transmission electron microscopy of experimentally deformed olivine crystals. In: *Flow and Fracture of Rocks* (edited by Heard, H. C., Borg, J. Y., Carter, N. L. & Raleigh, C. B.). *Am. geophys. Un. Geophys. Monogr. Ser.* **16**, 117–138.

Raleigh, C. B. 1967. Experimental deformation of ultramafic rocks and minerals. In: *Ultramafic and Related Rocks* (edited by Wyllie, P. J.). Wiley, New York, 191–199.

Raleigh, C. B. 1968. Mechanisms of plastic deformation of olivine. *J. geophys. Res.* **73**, 5391–5406.

Raleigh, C. B. & Kirby, S. H. 1970. Creep in the upper mantle. *Spec. Pap. miner. Soc. Am.* **3**, 113–121.

Raleigh, C. B. & Paterson, M. S. 1965. Experimental deformation of serpentinite and its tectonic implications. *J. geophys. Res.* **70**, 3965–3985.

Ramsay, J. G. 1980. The crack-seal mechanism of rock deformation. *Nature, Lond.* **284**, 135–139.

Reuber, I., Michard, A., Chalouan, A., Juteau, T. & Jermoumi, B. 1982. Structure and emplacement of the Alpine-type peridotites from Beni Bousera, Rif, Morocco: a polyphase tectonic interpretation. *Tectonophysics* **82**, 231–251.

Richter, F. & Voll, G. 1982. Deformation und Kristallisation bei alpiner Subduktion der Sesia-Zone des Val d'Aosta (N-Italien). *Fortschr. Miner.* **60**, 177–178.

Roeder, D. 1976. Die Alpen aus plattentektonischer Sicht. *Z. dt. geol. Ges.* **127**, 87–103.

Sander, B. 1930. Gefügekunde der Gesteine mit besonderer Berücksichtigung der Tektonite. Springer Verlag, Wien.

Streckeisen, A. L. 1967. Classification and nomenclature of igneous rocks. *Neues Jb. Miner. Abh.* **107**, 144–214.

Thayer, T. P. 1969. Peridotite–gabbro complexes as keys to petrology of mid-oceanic ridges. *Bull. geol. Soc. Am.* **80**, 1515-1522.

Toksöz, M. N., Minear, J. W. & Julian, B. R. 1971. Temperature field and geophysical effects of a downgoing slab. *J. geophys. Res.* **76**, 1113–1138.

Trommsdorff, V. 1982. Petrologic aspects of serpentinite metamorphism. *Rc. Soc. ital. miner. Petrol.* **38**, 549–559.

Trommsdorff, V. & Evans, B. W. 1974. Alpine metamorphism of peridotitic rocks. *Schweiz. miner. petrogr. Mitt.* **54**, 333–352.

Vogler, W. S. 1984. Alpine structures and metamorphism at the Pillonet Klippe—a remnant of the Austroalpine Nappe System in the Italian Western Alps. *Geol. Rdsch.* **73**, 175–206.

Vogler, W. S. & Voll, G. 1981. Deformation and metamorphism at the south-margin of the Alps, East of Bellinzona, Switzerland. *Geol. Rdsch.* **70**, 1232–1262.

Voll. G. 1960. New work on petrofabrics. *Lpool Manchr geol. J.* **2**, 503–567.

Voll. G. 1982. Gefüge-Entwicklung in der alpinen Subduktions zone. *Fortschr. Miner.* **60**, 210–212.

Voll. G. 1985. Fabric-development of peridotites and eclogites in subducted nappes of the western Alps. *Terra cognita* **5**, 437–439.

Wager, L. R. & Brown, G. M. 1968. *Layered Igneous Rocks*. Oliver & Boyd, Edinburgh.

Weissert, H. J. & Bernoulli, D. 1985. A transform margin in the Mesozoic Tethys: evidence from the Swiss Alps. *Geol. Rdsch.* **74**, 665–679.

Wicks, F. J. 1984. Deformation histories as recorded by serpentinites. I. Deformation prior to serpentinization. *Can. Miner.* **22**, 185–195.

Wicks, F. J. & Whittaker, E. J. W. 1977. Serpentinite textures and serpentinization. *Can. Miner.* **15**, 459–488.

Wicks, F. J., Whittaker, E. J. W. & Zussman, J. 1977. An idealized model for serpentine textures after olivine. *Can. Miner.* **15**, 446–458.

Williams, A. J. 1979. Foliation development in serpentinites, Glenrock, New South Wales. *Tectonophysics* **58**, 81–95.